ISOLATING THE OBSERVED INFLUENCE OF VEGETATION VARIABILITY OF LA PLATA RIVER BASIN ON THE CLIMATE OF SOUTH AMERICA

BY

DIVYANSH CHUG

THESIS

Submitted in partial fulfillment of the requirements
for the degree of Master of Science in Atmospheric Sciences
in the Graduate College of the
University of Illinois at Urbana-Champaign, 2018

Urbana, Illinois

Adviser:

Professor Francina Dominguez

ABSTRACT

Land surface variability and change can affect the overlying atmosphere through biogeophysical and biogeochemical feedbacks. The goal of our work is to isolate and quantify the local and remote influences of vegetation on the climate of South America using observational records. We find that the dominant mode of vegetation variability over the La Plata River basin in austral Spring is linked with warmer temperature and enhanced precipitation over central and south La Plata basin. A key aspect of this study is the use of remotely sensed land-surface characteristics alongside reanalysis data, and the use of the generalized equilibrium feedback assessment (GEFA) to isolate the effects of each forcing. The analysis uses a 34-year (1981-2014) record of the modified enhanced vegetation index (EVI2) from the NASA MEaSUREs Vegetation Index and Phenology dataset and the third generation normalized difference vegetation index (NDVI3g) from the Global Inventory Modeling and Mapping Studies. The dominant patterns of variability in space and time are analyzed using empirical orthogonal function/principal component (EOF/PC) analysis on a basin-wide scale. The dominant mode looks like a vegetation dipole, and can be explained using observed records of precipitation provided by the University of Delaware and the University of East Anglia Climate Research Unit. The second part of the study analyzes how these dominant modes of variability affect the overlying atmosphere at the continental scale. We use GEFA and its refinement, the stepwise GEFA, to statistically quantify the observed seasonal impacts of dominant terrestrial and oceanic forcings on the South American climate. This observed impact of vegetation on the seasonal accumulation of precipitation in the agricultural growing season holds crucial importance for the most heavily populated and economically active region of South America.

ACKNOWLEDGEMENTS

I take this opportunity to first and foremost thank my advisor, Prof. Francina Dominguez, for her never ending support, guidance and patience in shaping the first two years of my graduate studies. Prof. Dominguez has been an epitome of a motivated, committed and learned teacher who has never stopped to inspire great work. I could not have asked for a better advisor and mentor during my master's program, and I look forward to continue learning from her during my doctorate study.

Besides my advisor, I would like to thank Prof. Praveen Kumar for his encouragement, and insightful comments and questions. My sincere gratitude goes to Prof. Kaiyu Guan and Prof. Larry Di Girolamo, whose graduate-level courses allowed me to better understand the data and concepts employed for my research. I also thank Prof. Robert Trapp, Prof. Deanna Hence and Prof. Jeffrey Frame whose coursework has helped me greatly to transition from an engineering background into a meteorology program.

My sincere thanks goes to Dr. Zhao Yang, who has been a constant support as a senior group member and a friend, during my master's research. I thank my current and former labmates - Dr. Huancui Hu, Itinderjot Singh, Sujan Pal and Carolina Bieri, and coursemates - David King, Douglas Miller, Prateek Sharma and Randy Chase for all the fun during the last two years and for always being there whenever I needed them.

I cannot even begin to express my gratitude for my family and not run out of space here. My parents, Dr. Raj Chug (maa) and Ashok Kumar Chug (papa), have made me who I am today. I also thank Cadet Animesh Chug for being the perfect brother whose support and love has always instilled me with confidence. Everything leading up to the accomplishment of this thesis would not have been possible without them. Thank you.

Dedicated to my grandparents, Mrs. Krishna Chug and late Mr. Pari Ram Chug. They have always been the embodiment of discipline, liveliness and love.

TABLE OF CONTENTS

1. INTRODUCTION

Changes in the land surface, specifically in the terrestrial vegetation cover, can modulate the climate at different spatial and temporal scales [e.g., Dickinson & Henderson–Seller, 1998; Bonan 1997; Bounoua et al., 2000]. This complex two-way interaction is dominated by the atmosphere, through variations in precipitation, air temperature, wind intensity and direction, CO_2 concentration and solar radiation (Budyko 1974; Woodward 1987; Nemani et al. 2003; Woodward et al. 2004). As a response, the vegetation exerts a strong feedback on the atmosphere by modulating the exchanges of energy, moisture and momentum (biogeophysical feedbacks) and through processes that alter atmospheric CO_2 levels (biogeochemical feedbacks) (Pielke et al. 1998; Bonan 2002). Changes in vegetation modify the properties of the land surface – albedo, roughness length, root depth, stomatal resistance, etc. This has a direct effect on both biogeophysical and biogeochemical interactions, the local boundary layer, and eventually the processes that control precipitation (Stohlgren et al. 1998; Pielke et al. 2007). Additionally, the spatio-temporal heterogeneity of terrestrial vegetation results in land-atmosphere interactions across multiple scales, making it a complex phenomenon to completely observe and understand (Santanello, et al., 2018).

Numerical modeling studies to assess global-scale coupling relationships (e.g., soil moisture-precipitation coupling) has been a major focus of the climate community (Santanello et al., 2018). The most notable effort, the Global Land Atmosphere Coupling Experiment (GLACE; Koster et al. 2004, Koster et al. 2006, Guo et al. 2006) highlighted regions of strong coupling in GCMs where antecedent soil moisture had a significant influence on precipitation. Catalano et al. (2016) performed an analogous global-scale statistical analysis using observational data. Significant effort has also been devoted to the local-scale land-atmosphere interactions (Pan and

Mahrt 1987, Oke 1987, Diak 1990, Peters-Lidard and Davis 2000, Betts and Viterbo 2005, Santanello et al. 2005, 2007, Gentine et al. 2013), especially after the establishment of the Local Coupling (LoCo) working group supported by the Global Land-Atmosphere System Study (GLASS). Some studies have focused on the role of soil moisture anomalies or vegetation heterogeneity in inducing mesoscale circulations (Taylor et al. 2011, 2012; Hsu et al. 2017). However, there is a dearth of studies on vegetation feedbacks at the continental scale. Notable work includes vegetation feedback studies on North America (Wang et al. 2014), northern and tropical Africa (Wang et al. 2017; Yu et al. 2018) and Sahel (Yu et al. 2017) that apply a model validated statistical technique – the generalized equilibrium feedback assessment (GEFA) to observations and/or model output. In this study, we focus on the South American continent, and in particular on the La Plata River basin (LPRB).

The LPRB (14°-38° S, 43°-67° W) in southeastern South America is widely recognized as a hot-spot for land-atmosphere coupling where changes in the land surface can alter the atmospheric state and modulate the processes that control precipitation (Ruscica et al. 2015). The basin stretches over five countries – Argentina, Bolivia, Brazil, Paraguay and Uruguay, and is home to 50% of the combined population of these countries (Coronel et al. 2002). It is the second largest basin of South America after the Amazon. From an economic perspective, this region far exceeds the well-studied Amazon basin in hydroelectric power, agriculture and livestock, and supports 70% of combined Gross Domestic Product of these five nations (Coronel et al. 2002). Land-atmosphere interactions are important drivers of climate in the LPRB. Between 60% and 70% of the moisture that falls as mean annual precipitation over the LPRB comes from terrestrial sources (Dirmeyer and Brubaker 2007; Zemp et al. 2014; Martinez and Dominguez 2014), including 24% from the basin itself, and 20% from southern Amazon. The

dominant driver of precipitation in the northern part of the basin is the South American Monsoon (SAMS) (Marengo et al. 2010; Caffera and Berbery 2002). The exchanges of energy and water between vegetation-soil and the overlying atmosphere exert a strong influence on SAMS, mainly by modulating the continental heat gradient and consequently disrupting the continental scale circulation (Xue et al. 2006). Past studies focusing on the vegetation dynamics within South America have found significant activity in the terrestrial vegetation cover. The basins of La Plata and the Amazon have faced some of the highest deforestation rates during the past decades (Coronel et al. 2002, Nepstad et al. 2009, Hansen et al. 2013), and massive intensification of agriculture in the section of north LPRB encompassed by Brazil, with a decrease in the forested area from 90% to 20%, and an increase in the crop cover from near zero to 59% (Tucci and Clarke, 1998). Similar changes in the increase in crop cover through deforestation have been observed in the Paraguayan and Argentinian portions of the basin. Additionally, a large-scale shift in agricultural practices, specifically the shift to soybeans have been reported by Tucci and Clarke (1998), Paruelo et al. (2005) and by the Argentine Ministy of Agriculture Livestock and Fisheries in 2010. Barbosa et al. 2015 studied spatial patterns of vegetation and rainfall variability over the continent and found positive correlations in areas with both increase and decrease in vegetation.

The current understanding of the role of land surface in modulating the climate at large scales has largely been derived from numerical modeling studies (Santanello et al. 2018). A large number of those studies use land surface models coupled to atmosphere models, and perturb one or more aspects of the underlying land surface boundary conditions to observe the consequent changes in the system response (Koster 2004; Koster et al. 2006; Guo et al. 2006). Lee and Berbery (2012) found that replacement of the forests and savanna to crops in the LPRB causes

decreased moisture convergence and precipitation in the northern part of the basin, and increased convergence and precipitation to the south, demonstrating that the hydroclimatic response to sub-basin scale changes in the LPRB varies depending on the region. In terms of predictability, the importance of land surface has been demonstrated across all timescales from daily to seasonal (e.g., Koster et al. 2010, Hirsch et al. 2014, Dirmeyer and Halder 2016, Betts et al., 2017). For continental South America for instance, including appropriate representation of vegetation biophysical processes in numerical simulations results in an improved southward displacement of precipitation during the onset of the SAMS and a generalized better representation of precipitation (Xue et al. 2006). Moreover, the models applied in feedback studies range widely in terms of complexity and spatio-temporal resolution (Wang et al. 2014; Santanello et al. 2018).

However, several key limitations exist in the assessment of feedbacks using numerical models. While different models differ in their ability to represent the physical mechanisms that are responsible for changes in the system, the results also vary depending on the varied dynamical cores, physics, parameterizations and resolution. The sensitivity experiments are usually unrealistically extreme (e.g., complete deforestation, or completely replacing a specific vegetation type with bare ground or another vegetation type, etc.). However, differences in the spatial patterns in the land surface disturbance can completely change the resulting model response (D'Almeida et al. 2006; Mei and Wang 2009). The varied spatiotemporal scales across different studies tends to confound community thinking and consensus building (Guillod et al. 2015, Knist et al. 2016). Additionally, untangling the physical mechanisms responsible for the changes at the LA interface is not straight forward, and standard model outputs are often insufficient to diagnose coupled sensitivities. The aforementioned limitations give rise to the need of observational studies of land surface feedbacks.

In contrast to the abundance of modeling studies on vegetation feedbacks, studies using observational data have been rare (Kaufmann et al. 2003; Liu et al. 2006; Notaro et al. 2006; Wang et al. 2006, 2014; Catalano et al. 2016; Yu et al. 2017). The inadequate spatial and temporal coverage of observations in terms of both resolution and extent poses a challenge not only to the undertaking of such "ground-truth" studies, but also to evaluation and development of coupled LA models (Guillod et al. 2014). The adequacy of the observation network is also challenged due to the vast heterogeneity of the land surface, and the complexity and cost of addressing the required exhaustive set of variables across the soil-vegetation-atmosphere continuum. Santanello et al. (2018) pointed out that key land surface model parameters and state variables can be difficult to record routinely, or are unmeasurable given the current suite of observation network. Some studies have used observations to validate their results from large-scale modeling (Notaro and Liu, 2008; Santanello et al. 2009; Wang et al. 2013, 2014), or performed reanalysis-based quantification of the impacts of surface energy and moisture states on convective rainfall (Findell et al. 2011). However, land-atmosphere interactions remain a significant source of uncertainty in climate modeling (Flato et al. 2013).

Distinguishing the response of the atmosphere to changes in vegetation from the large atmospheric internal noise, and its isolation from the impact of other potential forcings (e.g. regional SSTs) poses a great challenge. The use of statistical techniques that can incorporate spatiotemporal variability, like granger causality (Granger 1969) and equilibrium feedback assessment (EFA; Frankignoul et al., 1998) limits the analysis to local feedback, and may not remove the impact of other forcings. The generalized equilibrium feedback assessment (GEFA; Liu et al. 2008; Liu and Wen 2008) overcomes some of the aforementioned challenges. It was developed to isolate the local and remote feedbacks of a single forcing in the presence of other

forcings. GEFA's capability in isolating the oceanic and terrestrial feedbacks on the North American climate has previously been demonstrated with observations as well as model output (Wang et al. 2013, 2014). Its refinement, the stepwise GEFA (SGEFA), uses akaike information criterion (AIC; Akaike, 1974) to first eliminate the negligible forcings from the GEFA feedback matrix. The selection of only the most important forcings further reduces the sampling error associated with the forcing matrix. SGEFA has been reliably employed and validated against GEFA as well as dynamical assessments for the North African climate (Yu et al. 2017, 2018; Wang et al. 2017). Given the capability of GEFA and SGEFA in isolating the local and remote impact of vegetation, it is a valuable tool for the current analysis.

The purpose of this study is to quantify and isolate the observed influence of monthly vegetation variability on the atmosphere across South America, with a focus on the impact on the seasonal climate of LPRB. This work involves the identification of the dominant forcings affecting the LPRB climate, and obtaining both the local and non-local feedbacks of the vegetation after excluding the feedback of SST variability. For LPRB, this represents a first attempt at assessing the regional atmospheric response to the land surface using observational data, and a step toward systematically narrowing down the mechanisms involved. The data and methods are introduced in the next section. Section 3 states the results from the analysis. The conclusions and further discussions are presented in section 4.

2. DATA AND METHODOLOGY

2.1 Data

The vegetation forcing in this study is represented by monthly-mean remotely sensed vegetation indices (VIs) from two different datasets. The first dataset is the normalized difference vegetation index (NDVI; Pinzon et al. 2005; Tucker et al. 2004, 2005) from the Global Inventory Modeling and Mapping Studies. This is the third generation NDVI from NOAA's series of Advanced Very High Resolution Radiometer (AVHRR) sensors, available from July 1981 – Dec 2016. This dataset hereon after is referred to as GIMMS NDVI. A major disadvantage of the ratio-based NDVI index is that it is susceptible to non-linearities, and asymptotic behavior (Didan et al. 2016). Additional drawbacks include saturation over high biomass regions such as forests (Huete 1997), and modulation by soil background conditions. For this reason we use a second dataset, the 2-band enhanced vegetation index (EVI2; Jiang et al. 2008; Didan et al. 2016) from the NASA Making Earth System Data Records for Use in Research Environments (MEaSUREs) Vegetation Index and Phenology (VIP) dataset. The 2-band adaptation of the EVI was designed to be compatible with EVI (Huete et al. 2006; Jiang et al. 2008) through backward extension to the AVHRR data record and forward compatibility with the latest Visible Infrared Imager/Radiometer Sensor (Welsch et al. 2001). This dataset, referred to as VIP EVI, is available for the entire duration of 1981-2014 (34 years). Together these products provide the longest continuous record of satellite based terrestrial vegetation. In addition to these two datasets, we employ the enhanced vegetation index (EVI; Running et al. 1994; Huete et al. 2002) from the collection-6 Moderate-resolution Imaging Spectroradiometer (MODIS) dataset (Didan et al. 2015) for validating the identification of the dominant vegetation forcing. MODIS collection-6 EVI (hereon after referred to as MOD6 EVI) is available from

2000-2017. Data for LPRB was extracted from all vegetation datasets and remapped to a 0.5° x 0.5° grid for further analysis. The length of the feedback analysis is limited to the years 1981-2014 which is the overlap period of the two longer term VI datasets (VIP EVI and GIMMS NDVI).

Monthly SSTs from the Hadley Center Sea Ice and Sea Surface Temperature (HadISST; Rayner et al. 2003) were used to represent the oceanic forcing. Observed air temperature and precipitation for terrestrial South America (SA) were extracted from the University of Delaware (UDEL; Willmott and Matsuura, 1995) and the University of East Anglia Climate Research Unit (CRU; Mitchell and Jones, 2005) datasets. Both datasets are available as monthly mean values since 1901 at a resolution of 0.5° x 0.5°. Geopotential height, wind, vertical integral of moisture flux (VIMF), vertically integrated moisture flux divergence (VIMFD), mean sea level pressure (MSLP) and vertical velocity were downloaded from the European Centre for Medium-Range Weather Forecast (ECMWF) Interim reanalysis (ERA-Interim) dataset at a resolution of 0.25° x 0.25°. Height, wind and VIMF were analyzed for a larger domain centered at SA (160°W-40°E and 15°N-60°S) and regridded to 0.5° x 0.5°. Data for site-specific surface fluxes of latent and sensible heat was downloaded from FLUXNET (http://fluxnet.fluxdata. org/) half-hourly observations. All data for this analysis, except surface heat fluxes was extracted for the years 1981-2014 and the seasonal cycle was removed to compute the anomaly field.

2.2 Methods

2.2.1 *Empirical orthogonal function (EOF) analysis*

We use EOF analysis (Obukhov 1947, 1960; Fukuoka 1951; Lorenz 1956; Kutzbach 1967; Preisendorfer 1988; Bretherton et al. 1992; Hannachi et al. 2007) to decompose the

spatiotemporal datasets of the forcing fields into structures that explain the maximum amount of variance. The analysis produces a set of patterns in the spatial dimension called empirical orthogonal functions (EOFs), and a complementary set of series in the time dimension knows as principal components (PCs).

2.2.2 *Generalized Equilibrium Feedback Assessment (GEFA)*

The current study uses GEFA (Liu et al. 2008; Liu and Wen 2008) and its refinement, stepwise GEFA (SGEFA; Yu et al. 2017, 2018; Wang et al. 2017) to isolate the feedback of terrestrial vegetation to the regional climate of LPRB. GEFA is first applied to assess the response of the atmosphere using observational data, which is later compared to the SGEFA response. The GEFA technique is based on the stochastic climate theory of Frankignoul and Hasselmann (1977). GEFA has the capability to isolate the impact of a slowly-evolving boundary forcing on the rapidly evolving atmosphere, in the presence of other forcings. It was developed to isolate both local and nonlocal feedbacks, and can be used with observations as well model output (Liu et al. 2008). While initially applied to SST forcing (Wen et al. 2010, Zhong et al. 2011 and Wang et al. 2013), GEFA has been successfully employed to isolate the feedback of vegetation on the atmosphere across North America (Wang et al. 2014), and Sahel rainfall (Yu et al. 2017).

The atmosphere at any time instant *t* is subject to variations due to its "rapid" internal variability and the "slow" boundary forcings from SSTs or vegetation cover. At timescales greater than or equal to a month, the change in the atmospheric variable can be decomposed into two terms as follows (Frankignoul et al. 1998; Liu et al. 2008):

$$A(t) = \mathbf{B} \times \mathbf{Y}(t) + N(t) \qquad (1)$$

where $A(t)$ represents the atmospheric variable at time t, **B** is the feedback matrix that we want to compute, $\mathbf{Y}(t)$ is a matrix of slowly evolving forcings, and $N(t)$ is the atmospheric internal noise. We can then multiply $\mathbf{Y}^{T}(t - \tau)$ on both sides and express the terms as covariance to yield:

$$\mathbf{C}_{A\mathbf{Y}}(\tau) = \mathbf{B}\mathbf{C}_{\mathbf{YY}}(\tau) + \mathbf{C}_{N\mathbf{Y}}(\tau) \qquad (2)$$

The superscript T represents the transpose, τ represents the lag time, and **C** is a covariance matrix between variables denoted by its subscript. Equation (5) states that the response of the atmosphere to slow-process forcings (e.g. SSTs, NDVI, etc.) at a lag time of τ, is a sum of the response of the "slow" and the "rapid" components to the same lagged forcings. The longest memory of the internal variability component is 1 week (Frankignoul and Hasselmann, 1977). Additionally, the internal variability of a future time cannot force oceanic or land surface variability. Based on this reasoning, the covariance of $\mathbf{Y}(t - \tau)$ with $N(t)$ is assumed to be zero. The feedback matrix **B** can then be computed as:

$$\mathbf{B} = \mathbf{C}_{A\mathbf{Y}}(\tau)\mathbf{C}_{\mathbf{YY}}(\tau)^{-1} \qquad (3)$$

Each vector of the feedback matrix **B** represents the response of the atmospheric variable *A* to a corresponding slowly varying forcing in the matrix **Y**. The units of **B** are: (unit of the atmospheric variable) (standard deviation of vegetation)$^{-1}$. The feedback strength can be quantified by multiplying **B** by the standard deviation of the corresponding forcing (e.g. SST, vegetation).

We perform GEFA in a truncated EOF space, using only the first few dominant modes of the forcing variables. For the oceanic forcing, the global ocean north of 60°S is divided into seven non-overlapping basins: north Atlantic ocean (NA; 20°–50°N, 100°W–20°E), tropical Atlantic ocean (TA; 20°S–20°N, 65°W–15°E), south Atlantic ocean (SA; 20°–60°S, 70°W–20°E), Indian ocean (I; 20°S–20°N, 35°–120°E), north Pacific ocean (NP; 20°– 50°N, 120°E–

100°W), tropical Pacific ocean (TP; 20°S–20°N, 120°E–60°W), and south Pacific ocean (SP; 20°–60°S, 120°E–70°W) (see Figure 1). EOF analysis is performed to extract the leading 2 modes from each basin. The vegetation forcing is extracted by applying EOF analysis to the VI datasets over the LPRB and validating against EOFs from the more reliable MOD6 dataset. Only the validated EOF pattern was chosen as a forcing for this analysis due to known issues with the longer-term datasets, e.g. errors induced due to multi-sensor nature of the dataset, AVHRR sensor degradation, etc. All the selected PCs (14 oceanic and 1 terrestrial) are combined into a single forcing matrix **Y**:

Y = [LPRB NA1 NA2 TA1 TA2 SA1 SA2 I1 I2 NP1 NP2 TP1 TP2 SP1 SP2]

where LPRB, 1 and 2 represent the PCs of the LPRB vegetation, the first and the second dominant mode of SST EOFs respectively. The statistical significance of GEFA is estimated using the Monte Carlo bootstrap approach (Czaja and Frankignoul, 2002, Wang et al. 2013, 2014; Yu et al. 2018) with 500 iterations. Finally, the seasonal GEFA feedback is computed as the average of the feedback strength from the individual calendar months.

2.2.3 *Stepwise selection*

Although the application of EOF analysis to perform GEFA in a truncated space reduces sampling errors, the short length of available observed datasets and large number of forcings can still generate substantial sampling errors (Wang et al. 2017). The stepwise GEFA (SGEFA) approach was developed to reduce this error by identifying a suitable subset of the full forcing matrix, by dropping the relatively less important forcings. An automatic selection routine using a forward selection approach (Hocking, 1976) was employed to achieve the subset selection. This approach has been utilized in previous studies to develop forecast models (Yin et al. 2014;

Segele et al. 2015; Yu et al. 2015). We follow a similar methodology prescribed by Wang et al. (2017) and Yu et al. (2017, 2018) to build a statistical prediction model. The relative quality of the model at every step of the forward selection is assessed using the Akaike information criteria (AIC; Akaike, 1974). We follow the procedure employed by Wang et al. (2017). First, for the system with N forcings, the vegetation forcing is fixed as the only component of the forcing matrix, and the GEFA feedback is calculated. This feedback is essentially the EFA feedback of LPRB vegetation to the atmospheric variable. The AIC of this model (AIC_1) is computed. Second, one additional forcing is added to the forcing matrix at a time, and the AIC corresponding to each of such (N-1) models is calculated. Third, the 2-forcing model corresponding to the lowest AIC value is selected and its AIC (AIC_2) is compared with that of the 1-forcing model (AIC_1). If AIC_2 is less than AIC_1, then the 2-forcing model is preferred. The same steps are repeated while adding one forcing at a time until no further addition is warranted by the AIC approach (i.e. minimum AIC of higher order models is greater than the AIC of the lower order model). This procedure is performed to generate the set of most important forcings for each grid cell in the atmospheric field. The first element of the feedback vector thus generated at each grid cell gives the feedback coefficient of the vegetation forcing at that location.

The fixing of a forcing, while defying the idea of "true" selection by AIC, is justified through performing a rigorous statistical significance assessment using the Monte Carlo bootstrap approach as described in the previous section. In principle, even if the vegetation forcing has been initialized as important at a location where it is unimportant, the statistical test will not show significance, thereby kicking the grid point out of the significant results (Yu et al.

2018). This approach makes sure there is a feedback value at each grid point, while producing similar results to the “free selection” approach employed by Yu et al. (2017).

3. RESULTS

EOF analysis has been widely employed to study the dominant spatio-temporal patterns of atmospheric variables (Obukhov 1947, 1960; Fukuoka 1951; Lorenz 1956; Hannachi et al. 2007) and SSTs (Lagerloef and Berstein, 1988; Keiner and Yan, 1997). In the oceanic basins, the leading EOFs provide a realistic representation of naturally occurring dominant modes of SST variability. In our analysis, we extracted the two dominant modes of variability for the seven oceanic sub-basins. The PCs of these fourteen leading modes are combined into a set of EOFs that represent the oceanic forcing.

3.1 Oceanic and Terrestrial Forcings

3.1.1 Oceanic Forcings

In this analysis, we highlight four of the fourteen oceanic modes extracted using EOF analysis. These modes represent oceanic spatial patterns that have been previously identified in the literature, and have a pronounced effect on the general circulation. Figure 1 shows the dominant SST EOFs of the tropical Pacific ocean (TP1), tropical Atlantic ocean (TA1), Indian ocean (I1) and north Pacific ocean (NP1), and their corresponding PCs for the August-November (ASON) season during the period 1981-2014. TP1 (Fig. 1a) represents the cold phase of El Niño Southern Oscillation (ENSO) mode – a La Niña pattern with the characteristic cold tongue feature in the central and eastern tropical Pacific (Philander 1990) explaining 56.82% of the variability. The corresponding PC series correlates significantly with the Oceanic Niño Index ($r = -0.935$, $p \sim 0$; not shown here). Its pronounced effect on the global circulation is well documented. TA1 is similar to the cold phase of tropical Atlantic Niño mode (Merle 1980; Zebaik 1993, Chang et al. 2006) explaining 42.60% of the variability. Apart from being a

moisture source for LPRB wet season precipitation (Martinez and Dominguez, 2014), many studies have indicated that tropical Atlantic has strong influence on the precipitation of tropical South America through interannual SST variability (Moura and Shukla, 1981; Hasternrath 1984; Nobre and Shukla, 1991). The dominant mode of the Indian Ocean (I1; 42.46%) represents the warm phase of Indian Ocean basin mode (Klein et al. 1999; Xie et al. 2002). The dominant mode in the north Pacific ocean (NP1) shows a horseshoe type pattern with cold anomalies along the Kuroshio-Oyashio extension region and warm anomalies surrounding it. This pattern represents the warm phase of the Pacific Decadal Oscillation (PDO) mode (Zhang et al. 1997; Mantua et al. 1997) explaining 28.20% of the variability, and the corresponding PC series is significantly correlated with the PDO index ($r = 0.935$, $p \sim 0$; not shown here).

3.1.2 Terrestrial Forcing

Past studies have successfully used GEFA to isolate the land surface feedback from that of oceanic forcings (Wang et al. 2014; Yu et al. 2017). These studies use time series of spatially averaged NDVI as the terrestrial forcing in the GEFA forcing matrix. However, the hydroclimatic response of LPRB to sub-basin scale land cover changes varies depending on the region (Lee and Berbery, 2011). For this reason, in this analysis we use sub-basin scale patterns of variability. In a similar manner as the oceanic forcing, EOF analysis provides a way to reduce the dimensionality of the data while retaining the spatial pattern.

We consider MOD6 EVI as a benchmark for validating the results from the longer term datasets. EOF analysis, applied to the monthly vegetation indices from the shorter MOD6 EVI dataset (2000-2017) reveal a dominant, basin-scale dipole mode of vegetation variability with a consistent spatial pattern for each month in the ASON season (fig. 2a). This mode explains

15.06% of the vegetation variability. The spatial pattern depicts a basin-wide dipole of vegetation anomalies with greening (positive VI anomalies) to the north and browning (negative VI anomalies) to the south. This pattern suggests a differential response of the northern and the southern parts of the basin, to the forcings that shape vegetation variability, in the years when this mode is active (characterized by high positive and low negative PC values). This mode is hereon after referred to as the La Plata vegetation dipole (LP1).

To generate a robust, dominant long term forcing for the GEFA framework, similar analysis was performed on the longer term vegetation datasets (VIP EVI and GIMMS NDVI) for the ASON season during 1981-2014. The identification of a long-term vegetation forcing was treaded carefully due to the multi-sensor nature of the datasets, known issues with the AVHRR reflectance data prior to 2000, and the difficulty in interpretation of EOFs since physical modes do not always have to follow the orthogonality constraint (Hannachi et al. 2007). The first dominant mode of VIP EVI dataset (not shown here) shows basin-wide greening, except for small regions of localized browning in the eastern and western parts of the basin centered around 20°S latitude. This mode explains 21.83% of the variability. However, this mode does not correspond to any of the first 3 dominant modes of MOD6 EVI that together explain 51.40% of the variability. Hence we do not choose this mode as the dominant vegetation forcing.

The second dominant mode from both the datasets (fig. 3) depicts a basin-wide dipole of vegetation anomalies, with greening to the north and browning to the south. The spatial structure of both the positive and the negative vegetation anomalies is consistent among all three datasets for the dipole mode, i.e. LP1. The PC series of this dipole mode from the three datasets are positively correlated (r-value between MOD6 EVI and VIP EVI is 0.96; between MOD6 EVI and GIMMS NDVI is 0.85) significant at the 95% confidence interval in the overlapping years of

2000-2014 (fig. 2b). In the analysis that follows, the PC time-series were detrended to remove any long-term signals, thus isolating the inter-annual variability, which is the focus of the analysis.

Natural modes of variability in the land surface have been relatively less explored than the ocean and atmosphere modes of variability. For this reason, we further analyze this dominant vegetation pattern. To investigate the possible first-order controls on the observed sub-basin scale vegetation variability, the LPRB was divided into 2 non-overlapping parts – north (NLRPB; 14°S-26°S, 43°W–60°W) and south (SLPRB, 26°S-38°S, 57°W–67°W). This division is consistent with the observed dipole. The division along 26°S is conveniently based on MODIS global land cover type data such that NLPRB mainly covers savannas/woody savannas and croplands, along with deciduous broadleaf forest toward the central LPRB region, whereas SLPRB primarily contains croplands and grasslands (not shown here; see Lee and Berbery, 2011). Figure 4 shows the lagged correlation led by precipitation (from UDEL dataset), between spatial average vegetation index for the month of September and spatial mean of monthly precipitation for the period 1981-2014 for NLPRB and SLPRB. The axis labels indicate the precipitation month. For example, *Sep* refers to the vegetation index and precipitation of the same month, i.e. September, whereas *Apr(-)* depicts the correlation between vegetation index of September and precipitation of April earlier in the same year. Other months in the season (August, October and November) show similar results. Vegetation in NLPRB responds positively and at short timescales (significant positive correlation coefficients for lag times of 0-2 months) to changes in precipitation. This suggests a rapid response of vegetation variability to precipitation forcing. Vegetation in SLPRB is strongly and significantly correlated with precipitation at the end of previous wet season. The peak of the correlation curve appears at a lag

of 5 months (April) significant at 95% confidence interval. Similar curves for all other months of the ASON season show similar behavior. MODIS collection-6 products (not shown here) also show similar results. This robust behavior adds to the physical meaningfulness of LP1. This also suggests a possible role of "soil memory" in shaping the sub-basin response, through soil water storage, particularly in the SLPRB. Analysis with CRU precipitation dataset also yields similar and consistent results as figure 4.

3.2 Tropical Pacific feedback

In this section, we describe how the GEFA analysis captures the feedback of tropical Pacific SSTs to the climate of the region. Assessment of the atmospheric response to SST variability over the tropical Pacific serves as a validation of GEFA and SGEFA's ability to represent the well-studied atmospheric response to ENSO in the presence of additional forcings. As shown in the EOF analysis, ENSO is the dominant mode of tropical pacific SSTs (TP1) and the forcing represents La Niña (Fig. 1a). We use all 15 forcings (14 oceanic + 1 terrestrial) and look at the GEFA response corresponding to TP1. The response is assessed over each atmospheric grid point in the domain 160°W-40°E and 15°N-60°S, while the terrestrial air temperature and terrestrial precipitation are analyzed over the continent. The feedback matrices (units: *atmospheric variable* per unit *forcing variable*) have been multiplied by the standard deviation of the forcing time-series (units: *forcing variable*) to quantify the feedback strength, i.e. the response pattern represents anomalies (units: *atmospheric variable*) in the respective variable as an isolated response to 1 standard deviation of the forcing mode.

Figure 5 shows the GEFA response of geopotential heights and winds at 250 hPa, heights at 850 hPa, VIMF, and terrestrial air temperature to a La Niña forcing. The upper-air response

shows weak troughing across the tropical Pacific with the strongest cyclonic anomalies off the western coast of SA, at the interface between the tropics and subtropics where the climatological subtropical jetstream exists. The higher latitudes exhibit increased heights with a wave-train like pattern, producing an anti-cyclonic anomaly over southern SA. This dipole pattern of anomalies reduces the climatological pressure gradient and favors the expected weakening of the subtropical jet during cold ENSO events (Kiladis and Mo, 1998). From a dynamic perspective, due to the enhanced subsidence over the central Pacific during La Niña conditions, the Hadley circulation can no longer maintain a strong subtropical jetstream (by the large-scale meridional flux of westerly momentum). This is evident in the strong easterly anomalies in the Pacific at the climatological position of the jet (centered around 30°S) indicating a weakening of the westerly jet (Fig. 5a). The anomalous troughing south of SA evident in the 250 hPa heights response, in the Bellingshausen sea region, has been observed as a robust feature in all seasons during cold ENSO events by Kiladis and Mo (1998). This feature along with increased heights over southern SA marks the poleward shift of the polar jetstream due to La Niña. Corresponding shifts in the frequency of cyclones due to this shift in the position of storm tracks related to ENSO have been found by Sinclair et al. (1997).

The lower atmosphere (850 hPa) response to La Niña (Fig. 5b) shows significant southeasterly anomalies of moisture flux over tropical and subtropical SA, with strongest anomalies centered around the tripoint between Bolivia, Brazil and Paraguay. The pattern is co-located with the climatological position of the South American Low-Level Jet and favors the weakening of the jet (Marengo et al. 2004). The South American Low-Level Jet brings moisture-laden winds from the north into LPRB. This reduced moisture flux into the region suggesting low-level divergence is in agreement with past studies (Ropelewski and Halpert 1987, 1989;

Aceituno 1988; Grimm et al. 1998; Grimm 2003; Grimm and Ambrizzi, 2009). The associated subsidence over the LPRB region leads to clear skies enabling more shortwave radiation to reach the surface, thereby increasing the net radiation absorbed by the surface. This is reflected in higher than normal temperature in central LPRB as captured by GEFA (Fig. 5c).

Figure 6 shows the GEFA and SGEFA response of precipitation over LPRB due to a La Niña forcing. Results from all the datasets consistently show a basin-wide reduction in precipitation over LPRB and enhanced precipitation over tropical Amazonia. The spatial agreement between the results suggests that GEFA and SGEFA are capturing a robust climate response to SST anomalies related to La Niña. In terms of magnitude, SGEFA seems to capture more realistic anomalies when compared to previous studies, with precipitation anomalies ranging between 1-2 mm/day (negative). This also shows the effectiveness of the AIC approach in reducing the error associated with GEFA. In conclusion, this technique recovers the classical atmosphere response to La Niña, which is characterized by the tropics-tropics and the tropics-extratropics teleconnections.

3.3 Feedback Response due to vegetation changes in the La Plata River Basin

3.3.1 Observed response

As shown in the EOF analysis, the terrestrial forcing represents a dipole anomaly in vegetation index characterized by greening over NLPRB and browning down of SLPRB. In this section, we analyze how the different atmospheric variables respond to this dominant mode of terrestrial forcing. Figure 7 shows the response of geopotential heights (850 hPa and 250 hPa), VIMF, 250-hPa winds, and terrestrial air temperature due to LP1. The 250-hPa pattern (fig. 7a) shows increased height anomalies over central and south LPRB with significant basin-wide anti-

cyclonic wind anomalies centered around 30°S off the Atlantic coast. The wave activity in the upper-air GEFA response resembles the non-local Rossby wave response to tropical sources of diabatic heating (Gill 1980; Hoskins and Karoly, 1981). The response of the lower atmosphere (fig. 7b) shows an increase in northerly moisture transport from the tropics into the LPRB, and a strengthening of the anti-cyclonic anomaly over the region of south Atlantic subtropical gyre that leads to an increase in the transport of northeasterly oceanic moisture into LPRB. The moisture flux anomalies maintain a northerly direction over the basin indicating the increased southward penetration of moisture into LPRB. The anomalous high pressure off the southeastern coast, apart from setting up an anti-cyclonic circulation that can increase the transport of oceanic moisture into LPRB, can also play a role in preventing the tropical moisture flux from exiting the LPRB from a northern latitude, thus supporting a north-south circulation across the basin.

The temperature response shows an increase in surface air temperature over central and south LPRB with the highest anomalies of 1.2°C. An interesting feature is the increase in temperature over north Argentina, encompassing the region dominated by the Northwestern Argentinian Low (NAL; Seluchi et al. 2003). Past studies have concluded that NAL is sensitive to augmentation of surface properties and a deepening of the NAL leads to an acceleration of the northerly flow across LPRB and changes in the intensity and position of precipitation (Ferreira et al. 2006).

Figure 8 shows the response of MSLP, VIMFD, and vertical velocity at 500 hPa. The MSLP (hPa anomaly) results show strong positive anomaly off the coast over the subtropical Atlantic and reduced surface pressure over southern South America, favoring a strong northerly circulation across the basin as seen in previous results. The response pattern of total column moisture flux divergence (kg m^{-2} s^{-1} anomaly) and 500 hPa vertical velocity (Pa s^{-1}) have been

analyzed over a smaller domain encompassing the LPRB. The 500 hPa level is chosen as the approximate level of non-divergence and strongest vertical motion on a synoptic scale. The results consistently show 3 centers of anomalously strong flux convergence (negative divergence) and upward motion (negative velocity in pressure units) over – a) central and western LPRB, b) Atlantic ocean southeast of LPRB, and c) southern LPRB.

Figure 9 shows the response of precipitation from 2 different forcing datasets, as evaluated using GEFA as well as SGEFA. The results show significant increase in precipitation over central and south LPRB as an isolated response to LP1. Both full and stepwise GEFA agree on the spatial pattern of the response. Similar to the response to TP1, SGEFA results are lower in magnitude than GEFA results. Results from the CRU dataset (not shown here) show consistent findings.

3.3.2 Proposed mechanism

The greening up of NLPRB (positive vegetation index anomalies) results in a reduction in surface albedo as greener, more dense vegetation darkens the surface as compared to sparse vegetation and/or bare ground. This would lead to an increase in the net radiation (R_N) at the surface, thus making more heat energy available for the surface sensible (H), latent (LE) and ground (G) heat fluxes. The resultant net column warming reduces the surface pressure and the moisture-laden winds from the Atlantic and the Amazon gush into the region. This increase in the moisture transport into the region is reflected in the response pattern of vertically integrated moisture flux (Fig. 7b). The change in the vegetation would alter the surface water budget through increased transpiration from the leaves. This would lead to an increase in LE and a reduction in the Bowen ratio. Segal et al. (1995) showed that a smaller Bowen ratio, with the

same value of R_N, leads to an increase in the thermodynamic potential for deep cumulus convection.

SLPRB behaves differently than NLPRB in terms of the distribution of energy at the surface due to its different land cover (mainly croplands and grasslands). The surface energy budget is largely dominated by latent heat flux as compared to sensible heat flux. The diurnal cycle of sensible and latent heat fluxes from 4 years (2009-2012) of Fluxnet data at Virasoro site (28°3´S, 56°5´W) in northeast Argentina and the area-averaged diurnal fluxes in SLPRB from WRF simulations done by Lee and Berbery (2011) both confirm this finding. A reduction in evapotranspiration and soil moisture as a result of the browning will significantly affect latent heat flux. The increase in local temperature due to LP1 in central and south LPRB thus indicates an increase in the sensible heat flux at the expense of latent heat flux to balance the net radiation at the surface. This anomalous heating leads to a warming of the boundary layer and a reduction in surface pressure (shown in fig. 8a, as MSLP feedback), thus breaking the thermodynamic barrier for southward transport of the moisture into SLPRB (shown in fig. 7b, as moisture flux feedback). The enhanced moisture can potentially come from all three sources – tropical Amazon, subtropical Atlantic and advection of increased evapotranspiration from NLPRB, and needs to be examined in future work. The induced northerly circulation is supported by the dipole feedback of MSLP (fig. 8).

The changes in NLPRB and SLPRB result in increased moisture transport into central and south La Plata. Additionally, the existing climatological convective instability (Zipser et al. 2006; Salio et al. 2007) is conditioned by increased sensible heat flux, thus providing a positive feedback to precipitation over the region, as an isolated response to the vegetation dipole (fig. 9). Notably, WRF sensitivity tests done by Ferreira et al. 2006 suggest that deepening of the NAL

by drier surface conditions led to a southward shift in the precipitation systems and in anomalous intensification of the rain over SLPRB.

The observational framework is limited by the availability of long-term accurate datasets. These results should be regarded as a first-order evidence of the existing link between land surface variability and seasonal climate. A more detailed modeling framework that incorporates the inter-annual variability of land surface is required to narrow down the exact mechanisms.

4. CONCLUSION AND DISCUSSION

The current study isolates the impact of the vegetation inter-annual variability across the LPRB on the climate of South America, using multiple observational datasets analyzed using the multi-variate statistical framework GEFA and stepwise GEFA (or SGEFA). This is a first observational evidence of the local and remote effects of LPRB vegetation on South American seasonal climate at a regional scale. This work builds on past understanding of land-atmosphere interactions that has come from numerical modeling studies, e.g., Lee and Berbery (2011). The assessment of vegetation feedback using observations is particularly challenging because the response of the atmosphere to vegetation is modest as compared to its internal variability, making it difficult to isolate. The presence of other forcings such as oceanic SSTs also influence the response. The short length of available datasets poses yet another limitation as the feedback response can be associated with large sampling errors. While past studies have assessed this response in a numerical modeling framework, this is a first attempt at understanding the local and remote influence of LPRB vegetation to the South American climate using observations. The identification of the vegetation forcing is accomplished using multiple satellite datasets. The dominant vegetation forcing, extracted using EOF analysis, consists of a dipole of vegetation anomalies with greening to the north and browning to the south of the LPRB. Lagged regional correlation analysis of vegetation indices with precipitation shows the differential sub-basin scale behavior of LPRB and adds to the physical meaning of the chosen EOF. The GEFA framework is first validated against the well-studied response to the ENSO forcing. The results, compared to past studies, clearly show the capability of this technique to isolate the response signal in the presence of other forcings. We apply the same framework to extract the vegetation feedback

using two different vegetation index datasets, as well as two different terrestrial precipitation datasets, for the austral Spring season (SON).

The results indicate a robust signal in the atmospheric response due to LPRB vegetation forcing during this season, characterized by both local and non-local effects. The greening up of NLPRB conditions the atmosphere for increased transport of moisture into the basin. This feedback is characterized by increase in net radiation at the surface and enhanced evapotranspiration. The browning of SLPRB modulates the surface energy distribution. The increased surface air temperature, due to the increase in sensible heat flux, leads to a decrease in surface pressure. This results in the deeper penetration of moisture into LPRB, and a precipitation surplus over central and southern parts of the basin. The impact on seasonal LPRB precipitation is of great importance for the region, as precipitation fuels hydroelectricity that along with rain-fed agriculture forms the backbone of the economy of the five countries within the LPRB. Our results also suggest significant wave activity in the upper atmosphere as an isolated response to LP1. Analysis of the upper-level wave activity is outside the scope of this paper.

It should be kept in mind that the current results are based on a linearity assumption of the GEFA and SGEFA statistical framework. In the real world, however, vegetation feedbacks can be non-linear (Zeng et al. 2002; Zhou et al. 2003). Higher-order effects and lag times greater than one month have not been explored yet. The spatial consistency between results from different datasets imparts confidence but further analysis is required to assess the accuracy of the magnitudes. The accuracy of this analysis is also limited by the errors in observations, and the short length of available data for a statistical analysis. Wang et al. (2014) showed that GEFA results using 25-year data contains large sampling errors. The current analysis addresses some of

the shortcomings pointed out in previous studies, e.g. the application of SGEFA overcomes some of the sampling errors through elimination of unimportant forcings. Furthermore, Richman (1986) and Hannachi et al. (2007) have reviewed a number of possible inherent disadvantages of unrotated PCs and EOFs when extracting individual modes of data variability in exploratory sciences. For example, Horel (1981) shows that if the first EOF has a constant sign over its domain, the second EOF generally exhibits a dipole nature with the zero line going through the maxima of the first EOF. The observed set of EOFs in this study case does not correspond to the orthogonality constraint pointed out by Horel (1981).

Future work would also need to address the relevance of other modes of vegetation variability, other seasons, higher order SST modes, and the impact of forcings other than SST and vegetation (e.g., Amazon vegetation). More importantly, narrowing down the exact mechanism of the modulation of the circulation at a continental scale and the southward enhancement of the northerly moisture flux by the observed vegetation dipole, and assessing the relative importance of different moisture sources, would be the focus of our future work. An advanced modeling framework such as the Advanced Research Weather Research and Forecasting model (Skamarock et al. 2005) combined with newly developed water vapor tracers (Insua-Costa and Miguez-Macho 2017, Miguez-Macho et al. 2013; Dominguez et al. 2017) can prove crucial in improving the hydroclimate predictability over the most heavily populated and economically active region of South America where seasonal forecasts are crucial for the prosperity of its 67 million inhabitants.

FIGURES

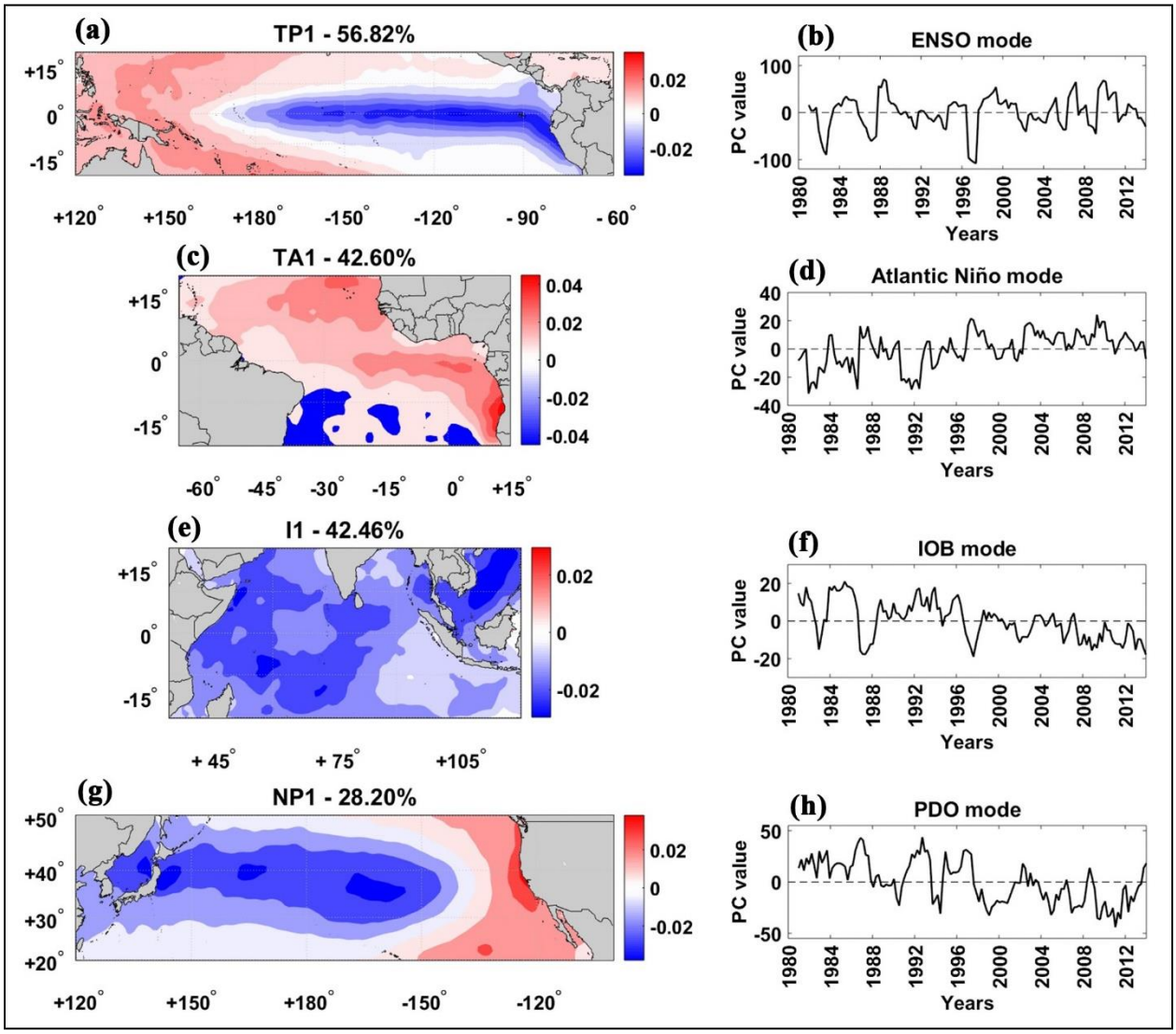

Fig. 1. Observed EOF1 (unitless) and PC1 (°C) of monthly (a)-(b) tropical Pacific, (c)-(d) tropical Atlantic, (e)-(f) Indian, and (g)-(h) north Pacific SSTs respectively.

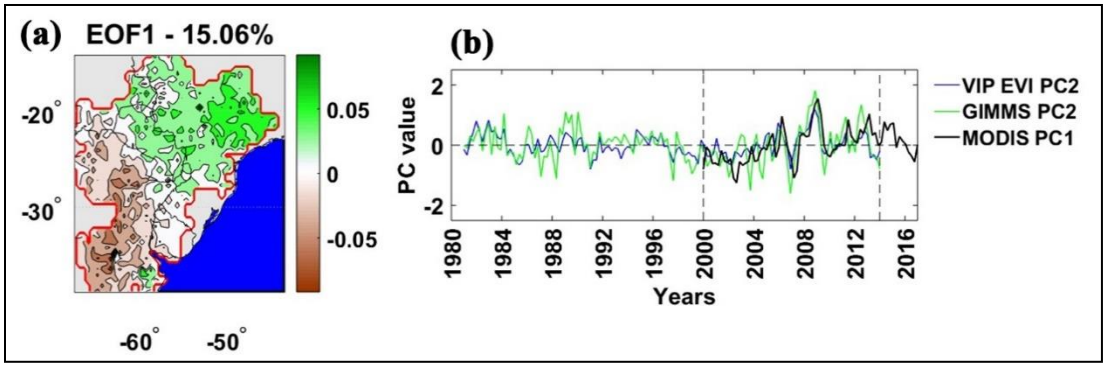

Fig. 2. (a) Observed EOF1 of monthly MODIS collection 6 EVI over LPRB in ASON season. (b) Corresponding PC1 from MODIS collection 6 dataset (black line), PC2 from VIP EVI (blue line) and PC2 from GIMMS NDVI (green line) for the same region and season. The latter two PC series constitute the dominant long-term vegetation forcing for this study.

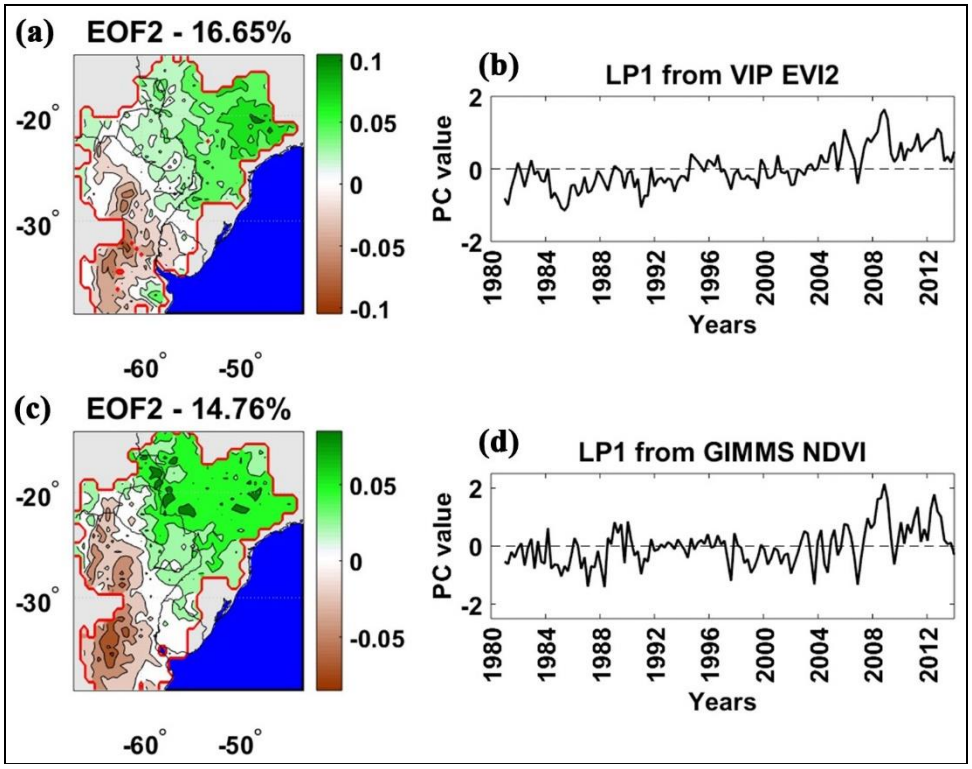

Fig. 3. Observed EOF2 and PC2 of monthly (a)-(b) VIP EVI, and (c)-(d) GIMMS NDVI respectively for ASON season over LPRB.

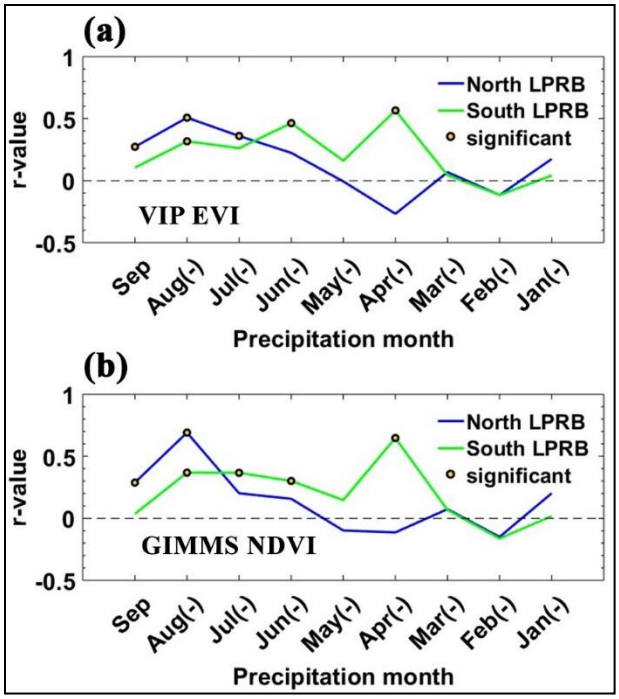

Fig. 4. Lagged correlation analysis for 34 years (1981-2014) of September regionally averaged vegetation index with lagged monthly precipitation over NLPRB [14°S-26°S, 43°W–60°W] and SLPRB [26°S-38°S, 57°W–67°W]; led by spatially averaged precipitation lagged successively by one month. Vegetation index from (a) VIP EVI, and (b) GIMMS NDVI dataset. Circular markers denote correlation values significant at the 95% confidence interval. Note the differential behavior of NLPRB and SLPRB, and the consistent behavior of the two datasets.

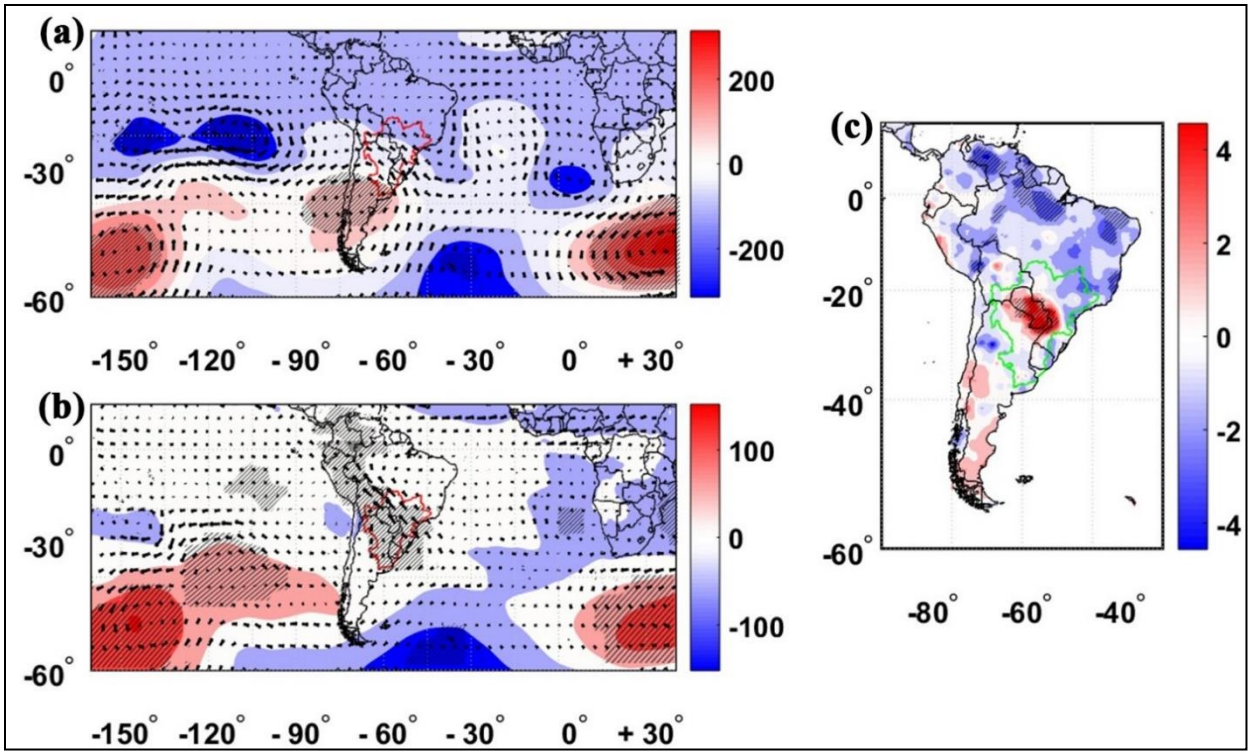

Fig. 5. Observed response pattern of (a) geopotential height (m) and wind (m s^{-1}) at 250 hPa, (b) geopotential height (m) at 850 hPa and vertical integral of moisture flux (kg m s^{-1}) from ERA-Interim Reanalysis dataset, and (c) terrestrial air temperature (°C) from the University of Delaware dataset, to La Niña forcing during SON. Hatching indicates 90% statistical significance based on Monte Carlo tests.

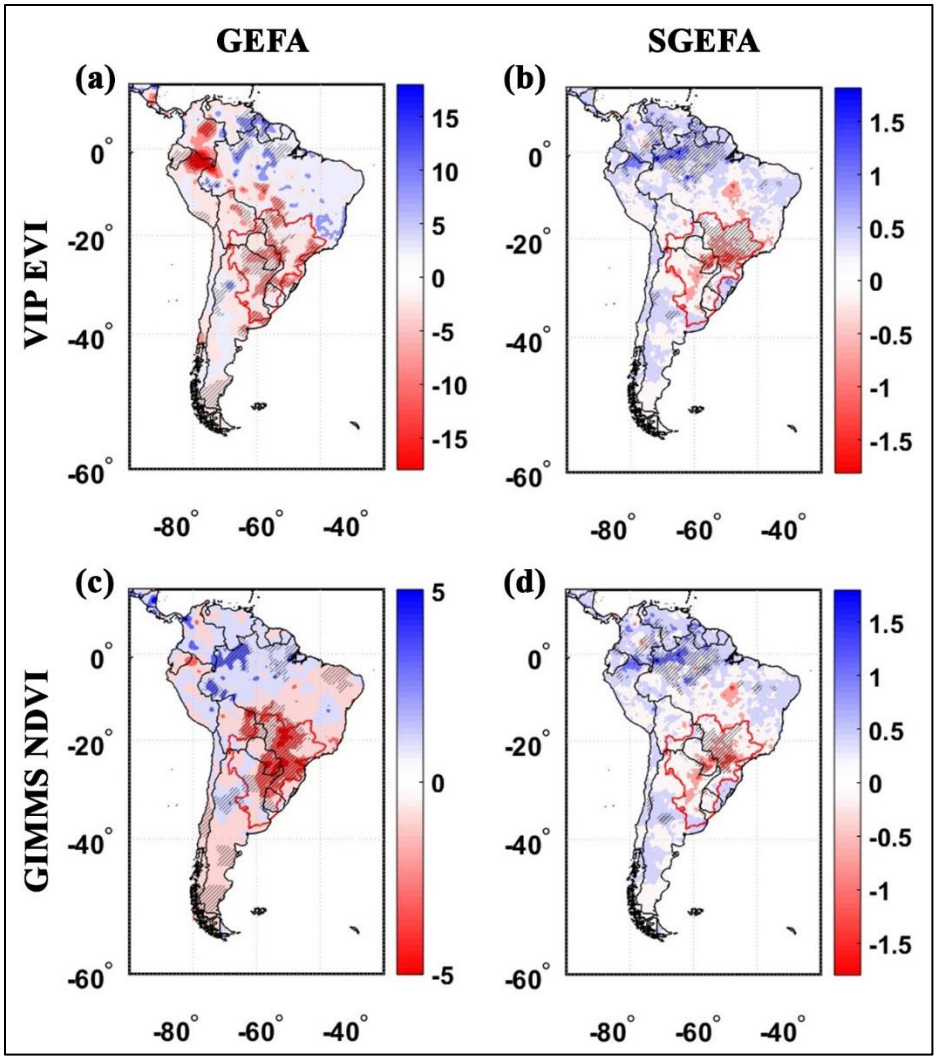

Fig. 6. Observed response pattern of precipitation (mm day^{-1}) to the La Niña forcing during SON using (a)-(b) VIP EVI, and (c)-(d) GIMMS NDVI vegetation index dataset; feedback isolated using full GEFA for (a),(c) and stepwise GEFA (or SGEFA) for (b),(d). Precipitation data obtained from the University of Delaware dataset. Hatching indicates 90% statistical significance based on Monte Carlo tests.

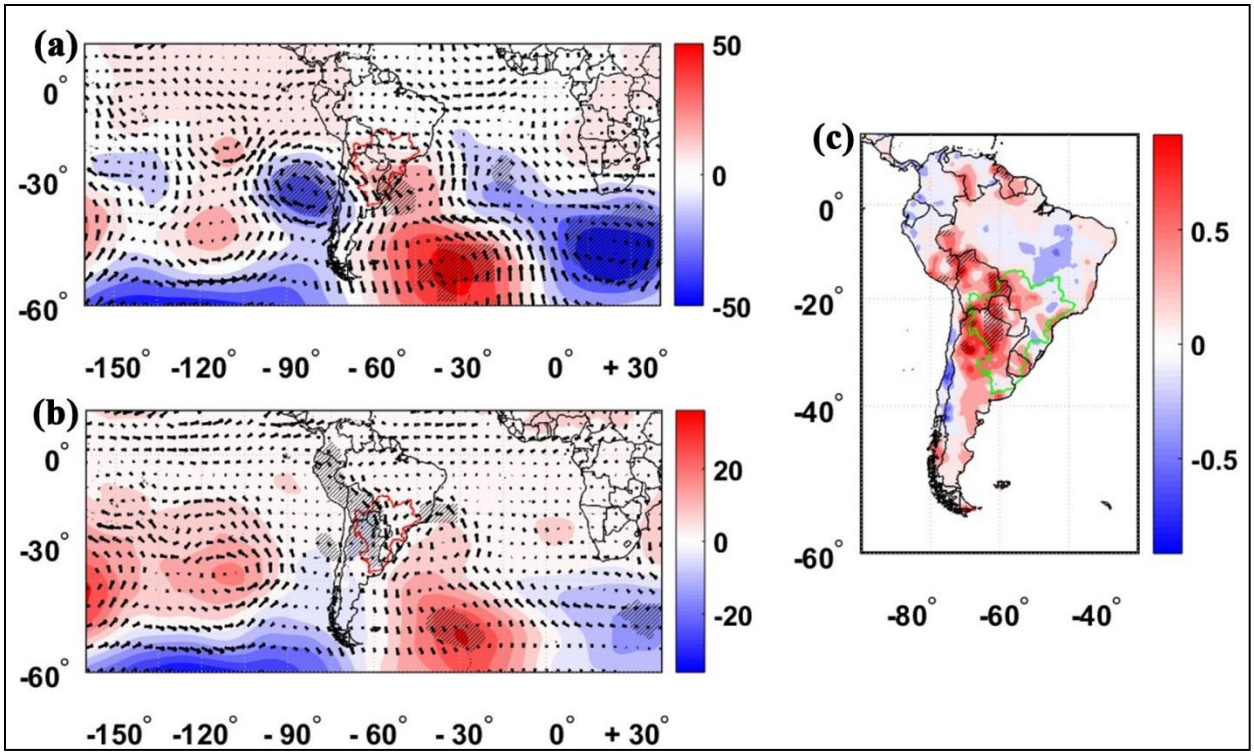

Fig. 7. Observed response pattern of (a) geopotential height (m) and wind (m s^{-1}) at 250 hPa, (b) geopotential height (m) at 850 hPa and vertical integral of moisture flux (kg m s^{-1}) from ERA-Interim Reanalysis dataset, and (c) terrestrial air temperature (°C) from the University of Delaware dataset, to LPRB vegetation forcing during SON. Hatching indicates 90% statistical significance based on Monte Carlo tests.

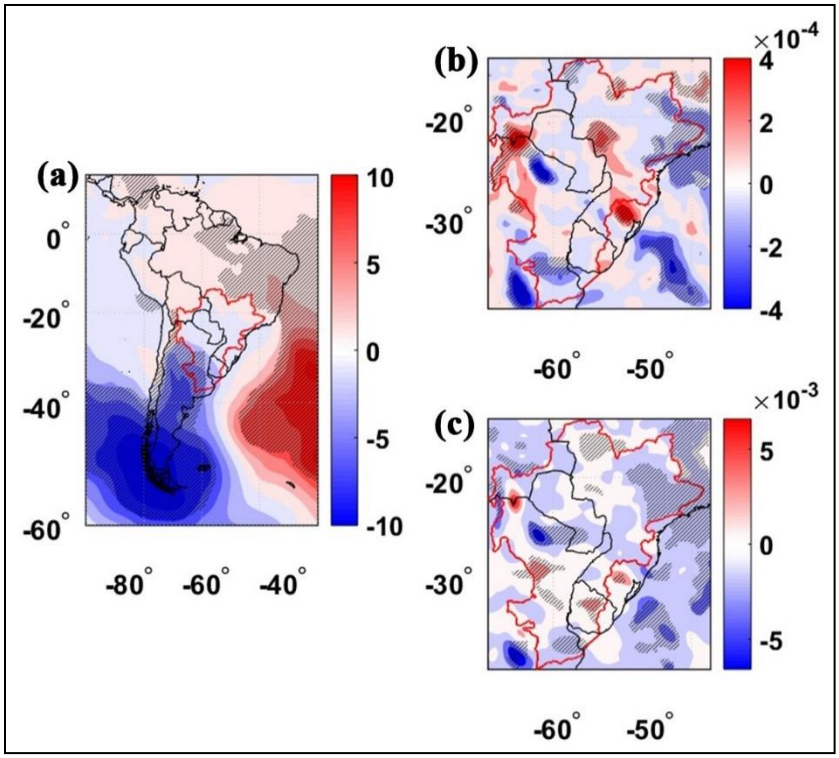

Fig. 8. Observed response pattern of (a) mean sea level pressure (hPa), (b) vertical integral of divergence of moisture flux (kg m^{-2} s^{-1}), and (c) vertical velocity (Pa s^{-1}) at 500 hPa from ERA Interim reanalysis dataset, to LPRB vegetation forcing during SON. Hatching indicates 90% statistical significance based on Monte Carlo tests.

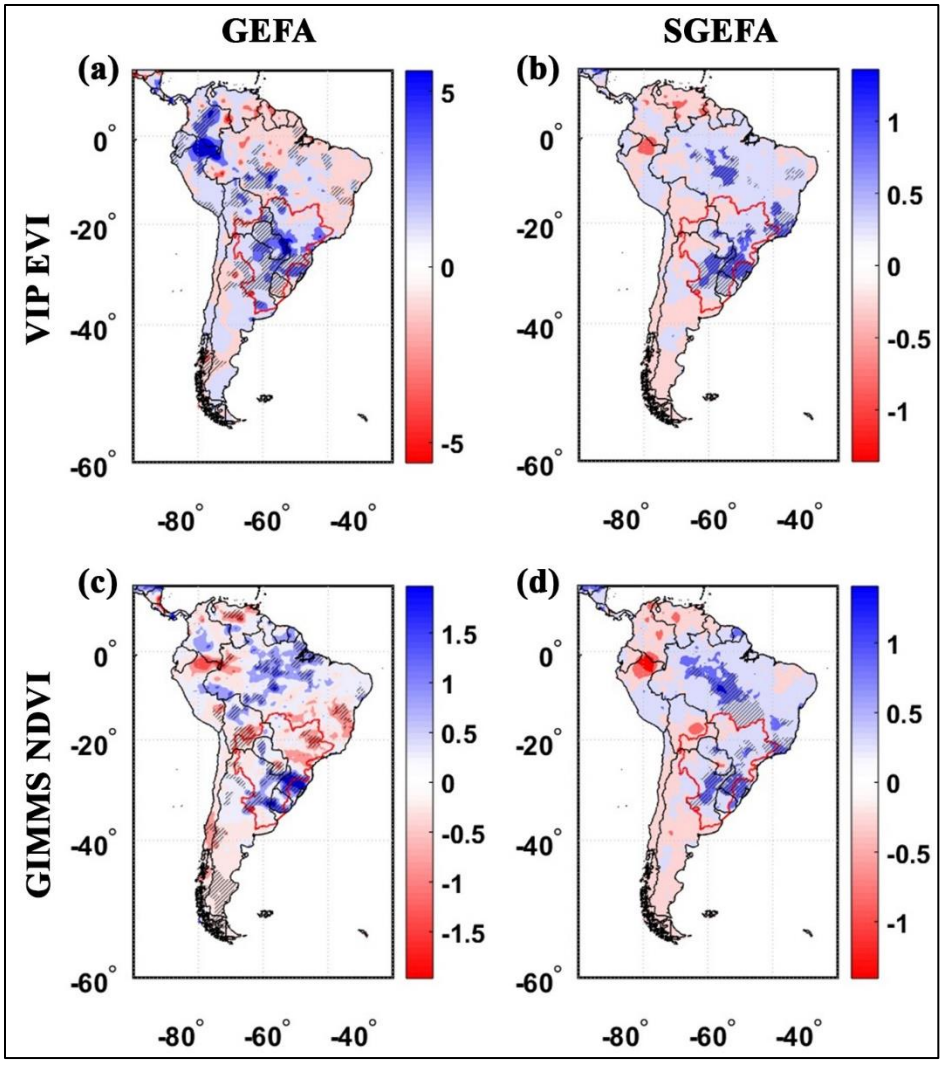

Fig. 9. Observed response pattern of precipitation (mm day^{-1}) to the LPRB vegetation forcing during SON using (a)-(b) VIP EVI, and (c)-(d) GIMMS NDVI vegetation index dataset; feedback isolated using full GEFA for (a),(c) and stepwise GEFA (or SGEFA) for (b),(d). Precipitation data obtained from the University of Delaware dataset. Hatching indicates 90% statistical significance based on Monte Carlo tests.

REFERENCES

Aceituno, P. (1988). On the functioning of the Southern Oscillation in the South America Sector Part I: surface climate. *Mon. Wea. Rev., 116*, 505–524.

Akaike, H. (1974). A new look at the statistical model identification. *IEEE Trans. Autom. Control, 19*, 716–723. doi:10.1109/TAC.1974.1100705

Argentine Ministry of Agri. Livestock & Fisheries. (2010). *Sistema Integrado de Informacion Agropecuaria.* Retrieved from http://www.siia.gov.ar

Barbosa, H., Kumar, T. L., & Silva, L. (2015). Recent trends in vegetation dynamics in the South America and their relationship to rainfall. *Nat. Hazards, 77*, 883. doi:10.1007/s11069-015-1635-8

Betts, A. K., & Viterbo, P. (2005). Land-surface, boundary layer, and cloud-field coupling over the southwestern Amazon in ERA-40. *J. Geophys. Res., 110*, D14108. doi:10.1029/2004JD005702

Betts, A. K., Tawfik, A. B., & Desjardins, R. L. (2017). Revisiting Hydrometeorology using cloud and climate observations. *J. Hydrometeor., 18*, 939-955.

Bonan, G. B. (1997). Effects of land use on the climate of the United States. *Clim. Change, 37*, 449-486.

Bonan, G. B. (2002). *Ecological Climatology: Concepts and Applications.* . Cambridge University Press.

Bounoua, L. e. (2000). Sensitivity of climate to changes in NDVI. *J. Climate, 13*, 2277–2292.

Bretherton, C. S., Smith, C., & Wallace, J. M. (1992). An Intercomparison of Methods for Finding Coupled Patterns in Climate Data. *J. Climate, 5*, 541–560. doi:10.1175/1520-0442(1992)005<0541:AIOMFF>2.0.CO;2

Budyko, M. I. (1974). *Climate and Life.* Academic Press.

Caffera, R. M., & Berbery, E. H. (2002). La Plata Basin Climatology. In *Climate Change in the La Plata Basin.* Inter American Institute on Global Change.

Catalano, F., Alessandri, A., De Felice, M., Zhu, Z., & and Myneni, R. B. (2016). Observationally based analysis of land–atmosphere coupling. *Earth Syst. Dynam., 7*, 251-266. doi:10.5194/esd-7-251-2016

Chang, P., Yamagata, T., Schopf, P., Behera, S. K., Carton, J., Kessler, W. S., . . . Xie, S. (2006). Climate Fluctuations of Tropical Coupled Systems—The Role of Ocean Dynamics. *J. Climate, 19*, 5122–5174. doi:10.1175/JCLI3903.1

Coronel, G., Menendez, A., & Chamorro, L. (2002). Physiography and Hydrology. In *Climate Change in the La Plata Basin.* Inter American Institute on Global Change.

Czaja, A., & Frankignoul, C. (2002). Observed impact of Atlantic SST anomalies on the North Atlantic Oscillation. *J. Climate, 15*, 606-623.

D'Almeida, C., Osmarty, C. J., Marengo, J. A., Hurtt, G. C., Dingman, S. L., & Keim, B. D. (2006). A water balance model to study the hydrological response to different scenarios of deforestation in Amazonia. *J. Hydrology, 331*, 125–136.

Diak, G. R. (1990). Evaluation of heat flux, moisture flux and aerodynamic roughness at the land surface from knowledge of the PBL height and satellite derived skin temperatures. *Agric. For. Meteor., 22*, 505–508.

Dickinson, R. E., & Henderson–Seller, A. (1998). Modeling tropical deforestation: A study of GCM land-surface parametrizations. *Quart. J. Roy. Meteor. Soc., 114*, 439-462.

Didan, K. (2015). MOD13Q1 MODIS/Terra Vegetation Indices 16-Day L3 Global 250m SIN Grid V006 [Data set]. *NASA EOSDIS LP DAAC.* doi:10.5067/MODIS/MOD13Q1.006

Didan, K., & Barreto, A. (2016). NASA MEaSUREs Vegetation Index and Phenology (VIP) Vegetation Indices Monthly Global 0.05Deg CMG [Data set]. *NASA EOSDIS Land Processes DAAC*. doi:10.5067/MEaSUREs/VIP/VIP30.004

Dirmeyer, P. A., & Halder, S. (2016). Sensitivity of surface fluxes and atmospheric boundary layer properties to initial soil moisture variations in CFSv2. *Wea. Forecast, 31*, 1973-1983. doi:10.1175/WAF-D-16-0049.1

Dirmeyer, P. A., & K. L. Brubaker. (2007). Characterization of the Global Hydrologic Cycle from a Back-Trajectory Analysis of Atmospheric Water Vapor. *J. Hydrometeor., 8*, 20.

Dominguez, F., Miguez-Macho, G., & Hu, H. (2016). WRF with Water Vapor Tracers: A Study of Moisture Sources for the North American Monsoon. *J. Hydrometeor., 17*, 1915-1927. doi:10.1175/JHM-D-15-0221.1

Ferreira, L. J., Saulo, C., Juan, R., & Seluchi, M. (2006). The Impact Of Land Use Changes Over The Low Level Circulation Related To The Northwestern Argentinean Low. *Proceedings of 8 ICSHMO* (pp. 1029-1035). Foz do Iguaçu, Brazil: INPE.

Findell, K. L., Gentine, P., Lintner, B. R., & Kerr, C. (2011). Probability of afternoon precipitation in eastern United States and Mexico enhanced by high evaporation. *Nature Geoscience, 4*, 434–439.

Flato, G., & Co-authors. (2013). Evaluation of Climate Models. In T. F. Stocker, & Co-editors (Eds.), *Climate Change 2013: The Physical Science Basis. Contribution of Working Group I to the Fifth Assessment Report of the IPCC* (pp. 741–866). Cambridge University Press.

Frankignoul, C., & Hasselmann, K. (1977). Stochastic climate models. Part II: Application to sea-surface temperature anomalies and thermocline variability. *Tellus, 29*, 289–305.

Fukuoka, A. (1951). A Study of 10-day Forecast (A Synthetic Report). *The Geophysical Magazine, 12*, pp. 177–218.

Gentine, P., Holtslag, A. A., D'Andrea, F., & Ek, M. (2013). Surface and atmospheric controls on the onset of moist convection over land. *J. Hydrometeor., 14*, 1443-1461.

Gill, A. E. (1980). Some simple solutions for heat-induced tropical circulation. *Quart. J. Roy. Meteor. Soc., 106*, 447–462. doi:10.1002/qj.49710644905

Granger, C. W. (1969). Investigating causal relations by econometric models and cross spectral models. *Econometrica, 37*, 424–438.

Grimm, A. M. (2003). The El Niño impact on the summer monsoon in Brazil: regional processes versus remote influence. *J. Climate, 16*, 263–280.

Grimm, A. M., & Ambrizzi, T. (2009). Teleconnections into South America from the Tropics and Extratropics on Interannual and Intraseasonal Timescales. In F. Vimeux, & Co-editors (Eds.), *Past Climate Variability in South America and Surrounding Regions, Developments in Paleoenvironmental Research.*

Grimm, A. M., Ferraz, S. E., & Gomes, J. (1998). Precipitation anomalies in Southern Brazil associated with El Niño and La Niña events. *J. Climate, 11*, 2863–2880.

Guillod, B. P., & Co-authors. (2015). Reconciling spatial and temporal soil moisture effects on afternoon rainfall. *Nature Communications, 6*, 6443.

Guillod, B., & Co-authors. (2014). Land-surface controls on afternoon precipitation diagnosed from observational data: uncertainties and confounding factors. *Atmos. Chem. Phys., 14*, 8343- 8367.

Guo, Z., & Co-authors. (2006). GLACE: The Global Land-Atmosphere Coupling Experiment. 2. Analysis. *J. Hydrometeor., 7*, 611-625.

Hannachi, A., Jolliffe, I. T., & Stephenson, D. B. (2007). Empirical orthogonal functions and related techniques in atmospheric science: a review. *Int. J. Climatol., 27*, 1119–1152. doi:10.1002/joc.1499

Hansen, M. C., Potapov, P. V., Moore, R., Hancher, M., Turubanova, S. A., Tyukavina, A., . . . Townshend, J. R. (2013). High-Resolution Global Maps of 21st-Century Forest Cover Change. *Science, 342*, 850-853.

Hasternrath, S. (1984). Interannual variability and annual cycle: mechanisms of circulation and climate in the tropical Atlantic. *Mon. Wea. Rev., 112*, 1097–1107.

Hirsch, A., Kala, J., Pitman, A., Carouge, C., Evans, J., Haverd, V., & Mocko, D. (2014). Impact of Land Surface Initialization Approach on Subseasonal Forecast Skill: A Regional Analysis in the Southern Hemisphere. *J. Hydrometeor., 15*, 300-319. doi:10.1175/JHM-D-13-05.1

Hocking, R. R. (1976). The analysis and selection of variables in linear regression. *Biometrics, 32*, 1–49. doi:10.2307/2529336

Horel, J. D. (1981). A rotated principal component analysis of the interannual variability of the Northern Hemisphere 500 mb height field. *Mon. Wea. Rev., 109*, 2080–2092.

Hoskins, B. J., & Karoly, D. J. (1981). The Steady Linear Response of a Spherical Atmosphere to Thermal and Orographic Forcing. *J. Atmos. Sci., 38*, 1179-1196. doi:10.1175/1520-0469(1981)038<1179:TSLROA>2.0.CO;2

Hsu, H., Lo, M.-H., Guillod, B. P., Miralles, D., & Kumar, S. (2017). Relation between precipitation location and antecedent/subsequent soil moisture spatial patterns. *J. Geophys. Res. Lett.* doi:10.1002/2016JD026042

Huete, A. R. (1997). A comparison of vegetation indices over a global set of TM images for EOS-MODIS. *Remote Sens. Environ., 59*, 440–451.

Huete, A., & Co-authors. (2006). VI White Paper. Retrieved from lcluc.umd.edu/products/Land_ESDR/index.asp

Huete, A., Didan, K., Miura, T., Rodriguez, E. P., Gao, X., & Ferreira, L. G. (2002). Overview of the radiometric and biophysical performance of the MODIS vegetation indices. *Remote Sensing of Environment, 83*, 195-213.

Insua-Costa, D., & Miguez-Macho, G. (2018). A new moisture tagging capability in the Weather Research and Forecasting model: formulation, validation and application to the 2014 Great Lake-effect snowstorm. *Earth Syst. Dynam.*, 167-185. doi:10.5194/esd-9-167-2018

Jiang, Z., Huete, A. R., Didan, K., & Miura, T. (2008). Development of a two-band enhanced vegetation index without a blue band. *Remote Sensing of Environment, 112*, 3833–3845. doi:10.1016/j.rse.2008.06.006

Kaufmann, R. K., Zhou, L., Myneni, R. B., Tucker, C. J., Slayback, D., Shabanov, N. V., & Pinzon, J. (2003). The effect of vegetation on surface temperature : A statistical analysis of NDVI and climate data. *Geophys. Res. Lett., 30*(22), 3–6. doi:10.1029/2003GL018251

Keiner, L. E., & Yan, X.-H. (1997). Empirical orthogonal function analysis of sea surface temperature patterns in the Delaware Bay. *IEEE Trans. Geosci. Remote Sens., 35*(5), 1299-1306.

Kiladis, G. N., & Mo, K. C. (1998). Interannual and Intraseasonal Variability in the Southern Hemisphere. Meteorology of the Southern Hemisphere. *Met. Monogr., Am. Met. Soc., 49*, 307–336.

Klein, S. A., Soden, B. J., & Lau, N.-C. (1999). Remote sea surface temperature variations during ENSO: Evidence for a tropical atmospheric bridge. *J. Climate, 12*, 917–932.
Knist, S., Goergen, K., Buonomo, E., Christensen, O. B., Colette, A., Cardoso, R. M., . . . Simmer, C. (2016). Land-atmosphere coupling in EURO-CORDEX evaluation experiments. *J. Geophys. Res. Atmos., 122*, 79-103. doi:10.1002/2016JD025476
Koster, R. D., & Co-authors. (2004). Regions of strong coupling between soil moisture and precipitation. *Science, 306*, 1138-1140.
Koster, R. D., & Co-authors. (2010). Contribution of land surface initialization to subseasonal forecast skill: First results from a multi-model experiment. *Geophys. Res. Lett., 37*, L02402. doi:10.1029/2009GL041677
Koster, R. D., & Co-authors, a. (2006). GLACE: The Global Land-Atmosphere Coupling Experiment. 1. Overview and results. *J. Hydrometeor., 7*, 590-610. doi:10.1175/JHM510.1
Kutzbach, J. E. (1967). Empirical eigenvectors of sea-level pressure, surface temperature,. *J. Appl. Meteorol., 6*, 791-802.
Lagerloef, G. S., & Bernstein, R. L. (1988). Empirical orthogonal function analysis of advanced very high resolution radiometer surface temperature patterns in Santa Barbara Channel. *J Geophys Res., 93*, 6863–6873.
Lee, S.-J., & Berbery, E. H. (2011). Land Cover Change Effects on the Climate of the La Plata Basin. *J. Hydrometeor., 13*, 84–102. doi:10.1175/JHM-D-11-021.1
Liu, Z., & Wen, N. (2008). On the assessment of nonlocal climate feedback. Part I: The generalized equilibrium feedback assessment. *J. Climate, 21*, 134-148.
Liu, Z., Notaro, M., Kutzbach, J., & Liu, N. (2006). Assessing global vegetation–climate feedbacks from observations. *J. Climate, 19*, 787–814.
Lorenz, E. N. (1956). *Empirical orthogonal functions and statistical weather prediction. Technical Report, Statistical Forecast Project Report 1.* MIT, Meteorology.
Mantua, N. J., Hare, S. R., Zhang, Y., Wallace, J. M., & Francis, R. C. (1997). A Pacific Interdecadal Climate Oscillation with Impacts on Salmon Production. *Bull. Amer. Meteor. Soc., 78*, 1069-1080. doi:10.1175/1520-0477(1997)078<1069:APICOW>2.0.CO;2
Marengo, J. A., Liebmann, B., Grimm, A. M., Misra, V., Dias, P. L., Cavalcanti, I. F., . . . Alves, L. M. (2010). Recent developments on the South American monsoon system. *International Journal Of Climatology, 32*, 1-21.
Marengo, J. A., Soares, W. R., Saulo, C., & Nicolini, M. (2004). Climatology of the Low-Level Jet East of the Andes as Derived from the NCEP–NCAR Reanalyses: Characteristics and Temporal Variability. *J. Climate, 17*, 2261–2280. doi:10.1175/1520-0442(2004)017<2261:COTLJE>2.0.CO;2
Martinez, J. A., & Dominguez, F. (2014). Sources of Atmospheric Moisture for the La Plata River Basin. *J. Clim., 27*, 6737–6753. doi:10.1175/JCLI-D-14-00022.1
Mei, R., & Wang, G. (2009). Rain follows logging in the Amazon? Results from CAM3–CLM3. *Climate Dynamics, 34*, 983–996.
Merle, J. (1980). Variabilité thermique annuelle et interannuelle de l'océan Atlantique équatorial Est. L'hypothèse d'un "El Niño" Atlantique. *Oceanol. Acta, 3*, 209–220.
Miguez-Macho, G., Rios-Entraza, A., & F. Dominguez. (2013). The Impact of Soil Moisture and Evapotranspiration Fluxes on the Spring Water Cycle in the Ierian Peninsula: a Study with Moisture Tracers in WRF. *AGU 2013 Fall Meeting.* San Francisco.

Mitchell, T. D., & Jones, P. D. (2005). An improved method of constructing a database of monthly climate observations and associated high-resolution grids. *Int. J. Climatol., 25*, 693–712.

Moura, A. D., & Shukla, J. (1981). On the dynamics of droughts in northeast Brazil: Observations, theory and numerical experiments with a general circulation model. *J. Atmos. Sci., 38*, 2653–2675.

Nemani, R. R., Keeling, C. D., Hashimoto, H., Jolly, W. M., Piper, S. C., Tucker, C. J., . . . Running, S. W. (2003). Climate-driven increases in global terrestrial net primary production from 1982 to 1999. *Science, 300*, 1560–1563.

Nepstad, D., Soares-Filho, B. S., Merry, F., Lima, A., Moutinho, P., . . . Stella, O. (2009). The End of Deforestation in the Brazilian Amazon. *Science, 326*, 1350–1351.

Nobre, P., & Shukla, J. (1991). Interannual variability of SST and wind stress over the tropical Atlantic and rainfall over Amazon and Northeast Brasil. *Fifth Conf. on Climate Variations. American Meteor. Soc., 1*, pp. 472–475. Denver, CO.

Notaro, M., & Liu, Z. (2008). Statistical and dynamical assessment of simulated vegetation feedbacks on climate over the boreal forests. *Climate Dyn., 31*, 691-712. doi:10.1007/ s00382-008-0368-8

Notaro, M., Liu, Z., & J.W.Williams. (2006). Observed vegetation–climate feedbacks in the United States. *J. Climate, 19*, 763-786.

Obukhov, A. M. (1947). Statistically homogeneous fields on a sphere. *Uspethi Mathematicheskikh Nauk, 2*, 196-198.

Obukhov, A. M. (1960). The statistically orthogonal expansion of empirical functions. *Bulletin of the Academy of Sciences of the USSR. Geophysics Series (English Transl.), 1*, 288–291.

Oke, T. R. (1987). *Boundary Layer Climates* (2 ed.). Routledge.

Pan, H. L., & Mahrt, L. (1987). Interaction between soil hydrology and boundary- layer development. *Bound. Layer Meteor., 38*, 185–202.

Paruelo, J. M., Guerschman, J. P., & Veron, S. R. (2005). Expansion agricola y cambios en el uso del suelo. *Cienc. Hoy, 15*(87), 14–23.

Peters-Lidard, C., & Davis, L. H. (2000). Regional flux estimation in a convective boundary layer using a conservation approach. *J. Hydrometeor., 1*, 170–182.

Philander, S. G. (1990). El Niño, La Niña, and the Southern Oscillation. Academic Press.

Pielke Sr, R. A., Avissar, R., Raupach, M., Dolman, A. J., Zeng, X., & Denning, A. S. (1998). Interactions between the atmosphere and terrestrial ecosystems: Influence on weather and climate. *Global Change Biol., 4*, 461–475.

Pielke, R. A., Adegoke, J., Beltra´n-Przekurat, A., Hiemstra, C. A., Lin, J., Nair, U. S., . . . Nobis, T. E. (2007). An overview of regional land-use and land-cover impacts on rainfall. *Tellus, 59B*, 587– 601.

Pinzon, J. E., Brown, M. E., & Tucker, C. J. (2005). Satellite time series correction of orbital drift artifacts using empirical mode decomposition. Hilbert–Huang Transform: Introduction and Applications. (N.Huang, Ed.) *World Scientific*, 167– 186.

Preisendorfer, R. W. (1998). *Principal Component Analysis in Meteorology and Oceanography.* Elsevier.

Rayner, N. A., Parker, D. E., Horton, E. B., Folland, C. K., Alexander, L. V., Rowell, D. P., . . . Kaplan, A. (2003). Global analyses of sea surface temperature, sea ice, and night marine

air temperature since the late nineteenth century. *J. Geophys. Res.*, *108*, 4407. doi:10.1029/2002JD002670
Richman, M. B. (1986). Rotation of principal components. *J. Climatol.*, *6*, 293-335.
Ropelewski, C. F., & Halpert, M. S. (1987). Global and regional scale precipitation patterns associated with the El Niño/Southern Oscillation. *Mon. Wea. Rev.*, *115*, 1606–1626.
Ropelewski, C. F., & Halpert, M. S. (1989). Precipitation patterns associated with the high index phase of the Southern Oscillation. *J. Climate*, *2*, 268-284.
Running, S. W., Justice, C. O., Salomonson, V., Hall, D., Barker, J., Kaufmann, Y. J., . . . Carneggie, D. (1994). Terrestrial remote sensing science and algorithms planned for EOS/MODIS. *International Journal of Remote Sensing*, *15*, 3587-3620. doi:10.1080/01431169408954346
Ruscica, R. C., A. A., S., & Menéndez, C. G. (2015). Pathways between soil moisture and precipitation in southeastern South America. *Atmospheric Science Letters*, *16*, 267–272. doi:10.1002/asl2.552
Salio, P., Nicolini, M., & Zipser, E. J. (2007). Mesoscale convective systems over southeastern South America and their relationship with the South American low-level jet. *Mon. Wea. Rev.*, *135*, 1290-1309.
Santanello, A. K., Friedl, M., & Ek., M. (2007). Convective Planetary Boundary Layer Interactions with the Land Surface at Diurnal Time Scales: Diagnostics and Feedbacks. *J. Hydrometeor.*, *8*, 1082- 1097.
Santanello, A. K., Friedl, M., & Kustas, W. (2005). Empirical Investigation of Convective Planetary Boundary Layer Evolution and its Relationship with the Land Surface. *J. Appl. Meteorol.*, *44*, 917-932.
Santanello, J., Dirmeyer, P., Ferguson, C., Findell, K. L., Tawfik, A. B., Berg, A., . . . Wulfmeyer, V. (2018). Land–Atmosphere Interactions: The LoCo Perspective. *Bull. Amer. Meteor. Soc.*, *99*, 1253–1272. doi:10.1175/BAMS-D-17-0001.1
Segal, M., Arritt, R. W., Clark, C., Rabin, R., & Brown, J. (1995). Scaling evaluation of the effect of surface characteristics on potential for deep convection over uniform terrain. *Mon. Wea. Rev.*, *123*, 383-400.
Segele, Z. T., Richman, M. B., Leslie, L. M., & Lamb, P. J. (2015). Seasonal-to-interannual variability of Ethiopia/Horn of Africa monsoon. Part II: Statistical multimodel ensemble rainfall predictions. *J. Climate, 28*, 3511–3536. doi:10.1175/ JCLI-D-14-00476.1
Seluchi, M., Saulo, A. C., Nicolini, M., & Satyamurty, P. (2003). The Northwestern Argentinean Low: A Study of Two Typical Events. *Mon. Wea. Rev.*, *131*, 2361-2378.
Sinclair, M. R., Renwick, J. A., & Kidson, J. W. (1997). Low-frequency variability of Southern Hemisphere sea level pressure and weather system activity. *Mon. Wea. Rev.*, *125*, 2531-2543.
Skamarock, W. C., Klemp, J. B., J. Dudhia, & Gill, D. O. (2005). A description of the advanced research WRF version 2.
Stohlgren, T. J., Chase, T. N., Pielke Sr, R. A., Kittel, T. G., & Baron, J. S. (1998). Evidence that local land use practices influence regional climate, vegetation, and stream flow patterns in adjacent natural areas. *Global Change Policy*, *4*, 495–504.
Taylor, C. M., de Jeu, R. A., Guichard, F., Harris, P. P., & Dorigo, W. A. (2012). Afternoon rain more likely over drier soils. *Nature*, *489*, 423-426.

Taylor, C. M., Gounou, A., Guichard, F., Harris, P. P., Ellis, R. J., Couvreux, F., & De Kauwe, M. (2011). Frequency of Sahelian storm initiation enhanced over mesoscale soil-moisture patterns. *Nature Geoscience, 4*, 430-433.

Tucci, C. E., & Clarke, R. T. (1998). Environmental issues in the La Plata Basin. *Water Res. Dev., 14*, 157–174.

Tucker, C. J., Pinzon, J. E., & Brown, M. E. (2004). Global inventory modeling and mapping studies. *Global Land Cover Facility, University of Maryland*.

Wang, F., Liu, Z., & Notaro, M. (2013). Extracting the dominant SST modes impacting North America's observed climate. *J. Climate, 26*, 5434–5452. doi:10.1175/JCLI-D-12-00583.1

Wang, F., Notaro, M., Liu, Z., & Chen, G. (2014). Observed local and remote influences of vegetation on the atmosphere across North America using a model-validated statistical technique that first excludes oceanic forcings. *J. Climate, 27*(1), 362–382. doi:10.1175/JCLI-D-13-00080.1

Wang, F., Notaro, M., Liu, Z., & Chen, G. (2014). Observed local and remote influences of vegetation on the atmosphere across North America using a model-validated statistical technique that first excludes oceanic forcings. *J. Climate, 27*, 362–382. doi:10.1175/JCLI-D-13-00080.1

Wang, F., Yu, Y., Notaro, M., Mao, J., Shi, X., & Wei, Y. (2017). Advancing a Model-Validated Statistical Method for Decomposing the Key Oceanic Drivers of Regional Climate : Focus on Northern and Tropical African Climate Variability in the Community Earth System Model (CESM). *J. Climate, 30*, 8517–8537. doi:10.1175/JCLI-D-17-0219.1

Wang, W., Anderson, B. T., Phillips, N., Kaufmann, R. K., Potter, C., & Myneni, R. B. (2006). Feedbacks of vegetation on summertime climate variability over the North American grasslands. Part I: Statistical analysis. *Earth Interact., 10*. doi:10.1175/ EI196.1

Welsch, C., Swenson, H., Cota, S., DeLuccia, F., Haas, J. M., Schueler, C., . . . Ardanuy, P. E. (2001). VIIRS (Visible Infrared Imager Radiometer Suite): a next-generation operational environmental sensor for NPOESS. *Geoscience and Remote Sensing Symposium, 2001. IGARSS'01. IEEE 2001 International, 3*, pp. 1020-1022.

Wen, N., Liu, Z., Liu, Q., & Frankignoul, C. (2010). Observed atmospheric responses to global SST variability modes: A unified assessment using GEFA. *J. Climate, 23*, 1739–1759.

Willmott, C. J., & Matsuura, K. (1995). Smart interpolation of annually averaged air-temperature in the United States. *J. Appl. Meteor., 34*, 2577–2586.

Woodward, F. I. (1987). *Climate and Plant Distribution.* Cambridge University Press.

Woodward, F. I., Lomas, M. R., & Kelly, C. K. (2004). Global climate and the distribution of plant biomes. *Philos. Trans. Roy. Soc. London, B359*, 1465–1476.

Xie, S.-P., Annamalai, H., Schott, F. A., & McCreary, J. P. (2002). Structure and mechanisms of south Indian Ocean climate variability. *J. Climate, 15*, 864–878.

Xue, Y., de Sales, F., Li, W. P., Mechoso, C. R., Nobre, C. A., & Juang, H. (2006). Role of Land Surface Processes in South American Monsoon Development. *J. Climate, 19*, 741–762. doi:10.1175/JCLI3667.1

Yin, L., Fu, R., Zhang, Y. F., Arias, P. A., Fernando, D. N., Li, W., . . . Bowerman, A. R. (2014). What controls the interannual variation of the wet season onsets over the Amazon? *J. Geophys. Res. Atmos., 119*, 2314–2328. doi:10.1002/2013JD021349

Yu, Y., Notaro, M., Liu, Z., Wang, F., Alkolibi, F., Fadda, E., & F.Bakhrjy. (2015). Climatic controls of the interannual to decadal variability in Saudi Arabian dust activity: Toward

the development of a seasonal prediction model. *J. Geophys. Res. Atmos., 120*, 1739–1758. doi:10.1002/2014JD022611

Yu, Y., Notaro, M., Wang, F., Mao, J., Shi, X., & Wei, Y. (2017). Observed positive vegetation-rainfall feedbacks in the Sahel dominated by a moisture recycling mechanism. *Nature Communications, 8*(1), 1-9. doi:10.1038/s41467-017-02021-1

Yu, Y., Notaro, M., Wang, F., Mao, J., Shi, X., & Wei, Y. (2018). Validation of a Statistical Methodology for Extracting Vegetation Feedbacks : Focus on North African Ecosystems in the Community Earth System Model. *J. Climate, 31*, 1565–1586. doi:10.1175/JCLI-D-17-0220.1

Zebiak, S. E. (1993). Air–sea interaction in the equatorial Atlantic region. *J. Climate, 6*, 1567–1586.

Zemp, D. C., Schleussner, C.-F., Barbosa, H. M., van der Ent, R. J., Donges, J. F., Heinke, J., . . . Rammig, A. (2014). On the importance of cascading moisture recycling in South America. *Atmos. Chem. Phys., 14*, 13337–13359. doi:10.5194/acp-14-13337-2014

Zeng, N., Hales, K., & Neelin, J. D. (2002). Nonlinear Dynamics in a Coupled Vegetation–Atmosphere System and Implications for Desert–Forest Gradient. *J. Climate, 15*, 3474–3487.

Zhang, Y., Wallace, J., & Battisti, D. (1997). ENSO-like Interdecadal Variability: 1900–93. *J. Climate, 10*, 10.1175/1520-0442(1997)010<1004:ELIV>2.0.CO;2.

Zhong, Y. F., Liu, Z. Y., & Notaro, M. (2011). A GEFA assessment of observed global ocean influence on U.S. precipitation variability: Attribution to regional SST variability modes. *J. Climate, 24*, 693–707.

Zhou, L., Kaufmann, R. K., Tian, Y., Myneni, R. B., & Tucker, C. J. (2003). Relation between interannual variations in satellite measures of northern forest greenness and climate between 1982 and 1999. *J. Geophys. Res., 108*, 4004. doi:10.1029/2002JD002510

Zipser, E. J., Cecil, D. J., Liu, C., Nesbitt, S. W., & Yorty, D. P. (2006). Where are the most intense thunderstorms on Earth? *Bull. Amer. Meteor. Soc., 87*, 1057–1071.